Supplementary Information for:

Live imaging of ferrous iron dyshomeostasis in ageing *Caenorhabditis elegans*

Simon A. James, Blaine R. Roberts, Dominic J. Hare, Martin D. de Jonge, Ian E. Birchall, Nicole L. Jenkins, Robert A. Cherny, Ashley I. Bush and Gawain McColl

Supplementary Table 1: New strains used in this study.

Name	**Genotype**	**Reference**
GMC005	*ftn-2*(*ok404*) I ; *ftn-1*(*ok3625*) V	This study
GMC006	*ftn-2*(*ok404*) I ; *daf-2*(*e1370*) III	This study
GMC007	*ftn-2*(*ok404*) I ; *daf-2*(*e1370*) III ; *ftn-1*(*ok3625*) V	This study

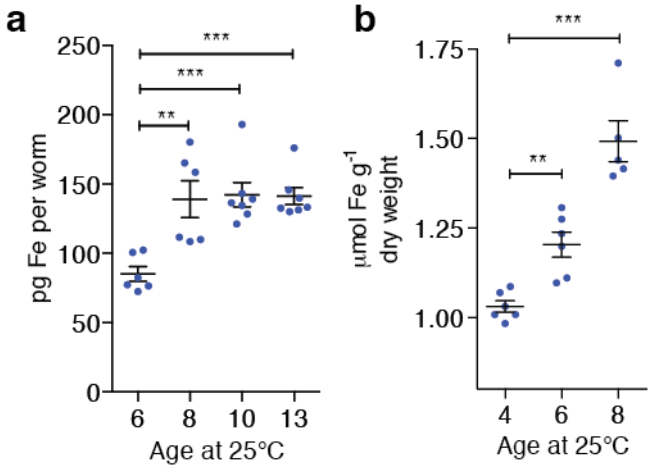

Supplementary Figure 1: (**a**) Bulk iron levels measured by ICP-MS from aging cohorts of wild type (shown is mean total iron per worm ± SEM, 100 animals per measure). (**b**) Bulk iron levels (measured via ICP-MS) from aging cohorts of wild type (shown is mean µmol iron per dry weight ± SEM; ** $p<0.01$, *** $p<0.001$, 2-tailed *t*-test).

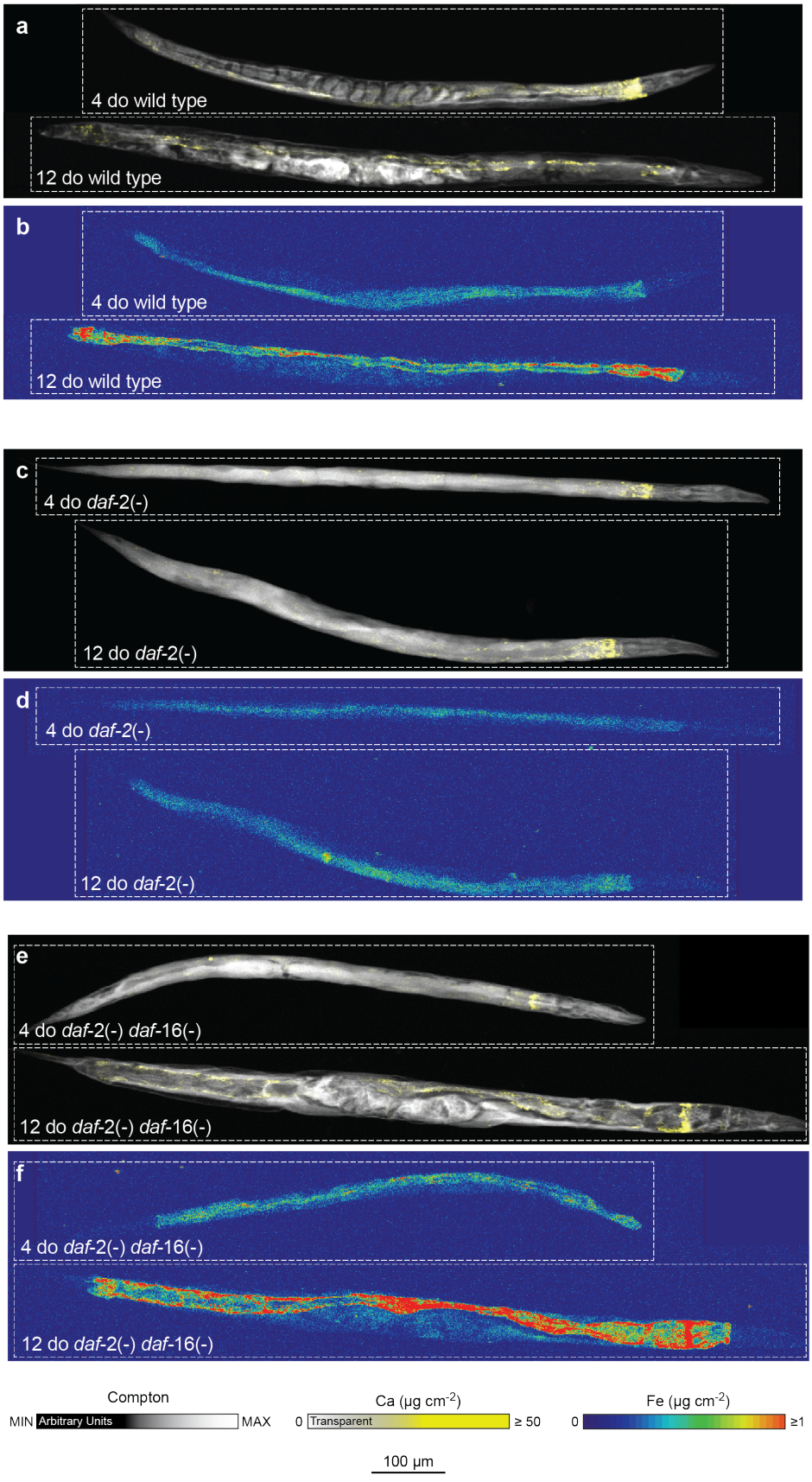

Supplementary Figure 2: Representative X-ray fluorescence micrographs of wild type, *daf-2(-)* and *daf-2(-):daf-16(-)* adult *C. elegans* (4- and 12-day old). (**a**), (**c**), (**e**)

Inelastic scatter of incident photons (Compton scatter) provides anatomical visualization (greyscale), and intestinal cells are highlighted by calcium (yellow). (**b**), (**d**), (**f**) While considerable age-related increases in the iron load were observed for wild type animals and short lived *daf-2(-):daf-16(-)* the *daf-2* mutants show a very minor increase in iron load over lifespan along with good anatomical preservation.

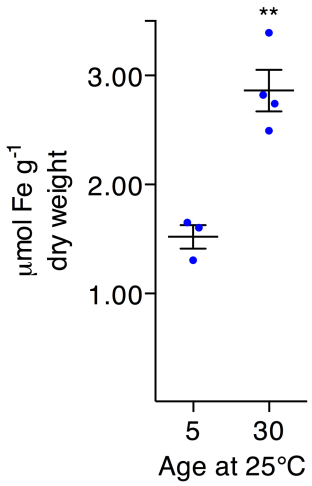

Supplementary Figure 3: Bulk iron levels (measured via ICP-MS) from young (5-day old) versus 30-day old *daf-2*(*e1370*) animals (shown is mean µmol iron per dry weight ± SEM; ** $p<0.01$, 2-tailed *t*-test).

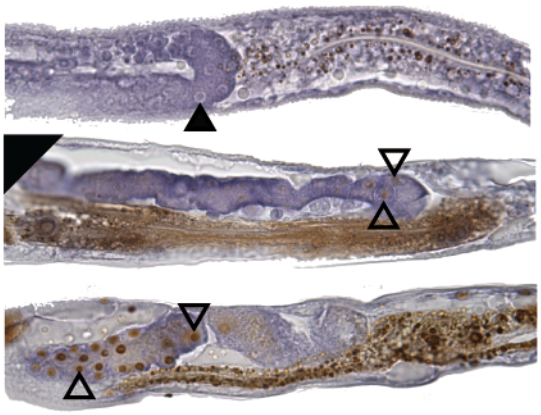

Supplementary Figure 4: Histological staining for Fe (brown) in young (4-day, *top*), post-reproductive (8-day, *middle*) and old (12-day, *bottom*) *C. elegans*. Mid-body sections distal gonad nuclei free of iron in young adults (solid triangles). Aged individuals have increasing ectopic iron deposits within the germline nuclei (open triangles).

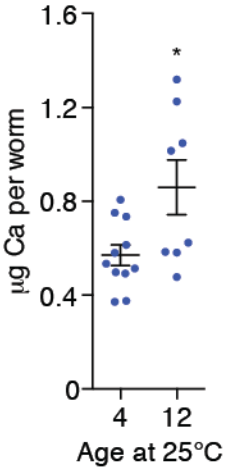

Supplementary Figure 5: Total calcium increases with age in wild type (p<0.05, 2-tailed t-test). Shown are mean ± SEM from age matched individual XFM images.

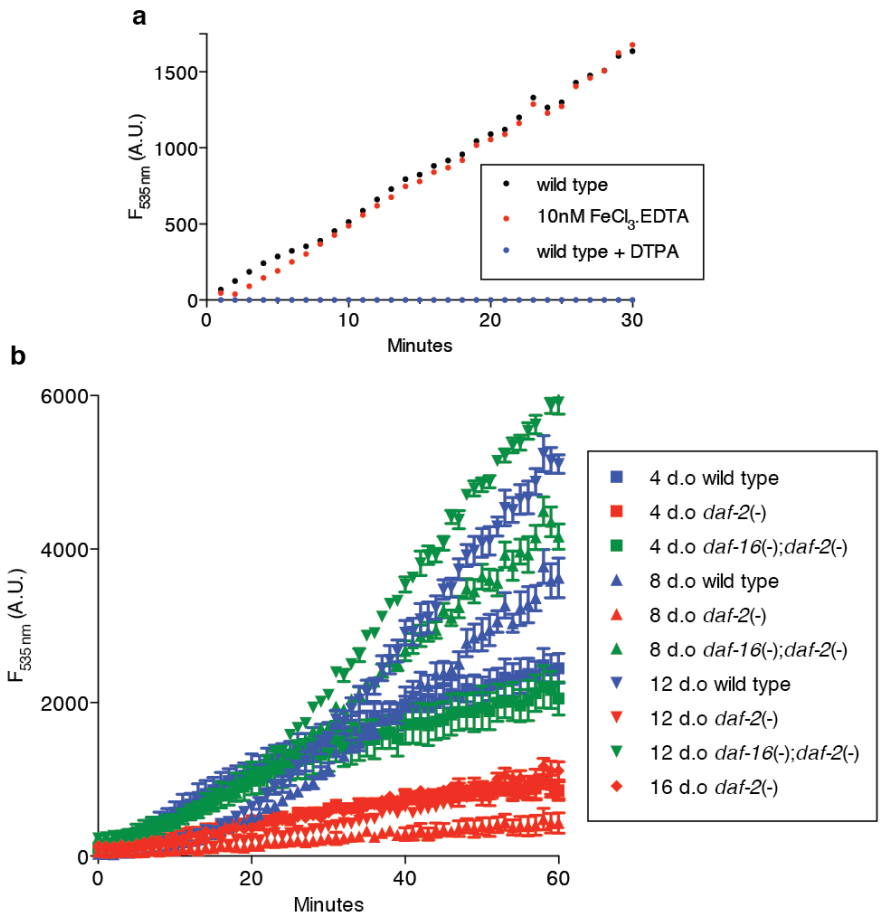

Supplementary Figure 6: *Ex vivo* DCF validation. (**a**) ROS production detected by DCF fluorescence from lysates of young adult wild type *C. elegans* (10µg), including a positive control of 10 nM $FeCl_3$.EDTA. ROS production was silenced by addition of 50 µM diethylenetriamine penta-acetic acid (DTPA). (**b**) DCF fluorescence increasing over time in lysates from 4, 8, 12 and 16-day old wild type, *daf-2*(-) and *daf-16*(-);*daf-2*(-) animals.

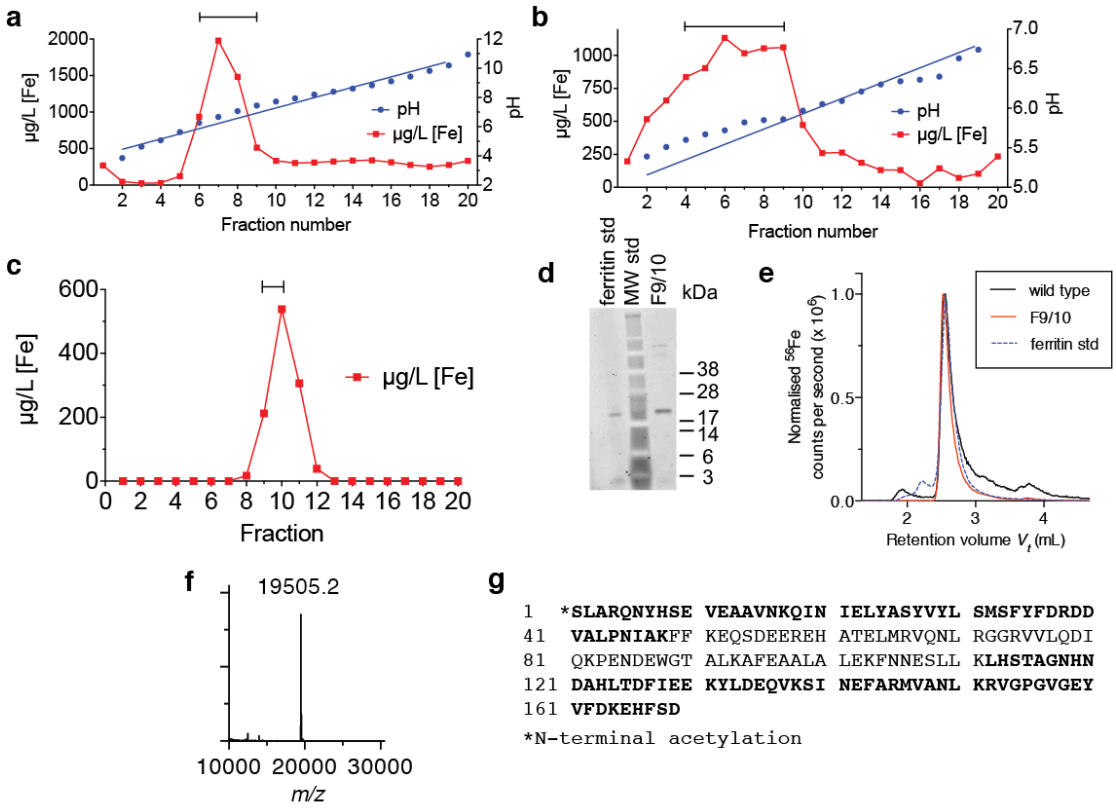

Supplementary Figure 7: Purification of native *C. elegans* ferritin. Since Peak #2 (**Fig. 3a**) is the major iron fraction at all ages, to identify the main protein component of this peak a large number of animals of mixed ages were pooled. 10g of soluble fraction of *C.* elegans lysate was applied to (**a**) isoelectric focusing (pH 3-10) and separated fractions were measured for iron content by atomic absorption spectroscopy. Fractions 6-8 were pooled and refocused. (**b**) Fractions 4-9 were collected from a narrower isoelectric refocusing (pH 5-7). (**c**) Native size exclusion of pooled samples resolved a iron containing peak. Fractions 9 and 10 (F9/10) were pooled for further analysis via immunoblotting and mass spectrometry. (**d**) Oriole stained SDS-PAGE of (1) Horse ferritin, 2) Protein size standards and 3) F9/10, showing a protein species in F9/10 resolving at ~19 kD. (**f**) LC-ICP-MS of lysate from wild type *C. elegans* (starting material), F9/10 and Horse ferritin showing co-elution of native horse ferritin and material in F9/10. (**g**) MALDI MS of identifies a single parent species of 19505.2 Da in F9/10 purified *C. elegans* FTN-2. (*H*) MALDI-MS/MS of lysC-digested F9/10 identifies protein as FTN-2 (62% sequence coverage over 6 fragments, Mascot score of 136, p =2.3x10^{-5}). Shown in bold are the residues in the identified fragments of FTN-2 identified residues. Note the starting methionine has been cleaved and the mature protein has a N-terminal acetylation.

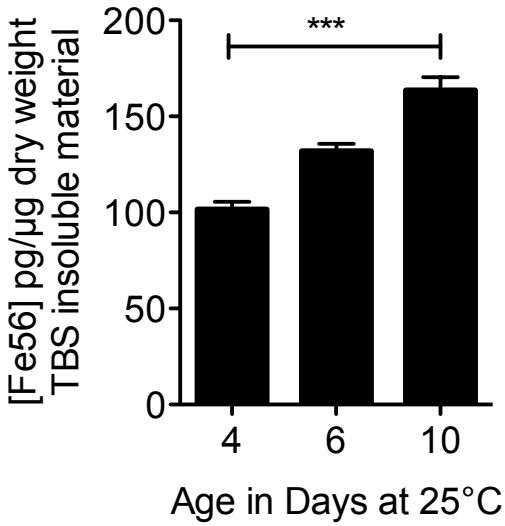

Supplementary Figure 8: Insoluble iron increases in aging wild type *C. elegans*. Shown are bulk iron measures of Fe56 per unit dry weight of the Tris-buffered saline (TBS) insoluble fraction from aged cohorts of wild type (mean from triplicate measures ± SEM; *** $p<0.001$, 2-tailed *t*-test).

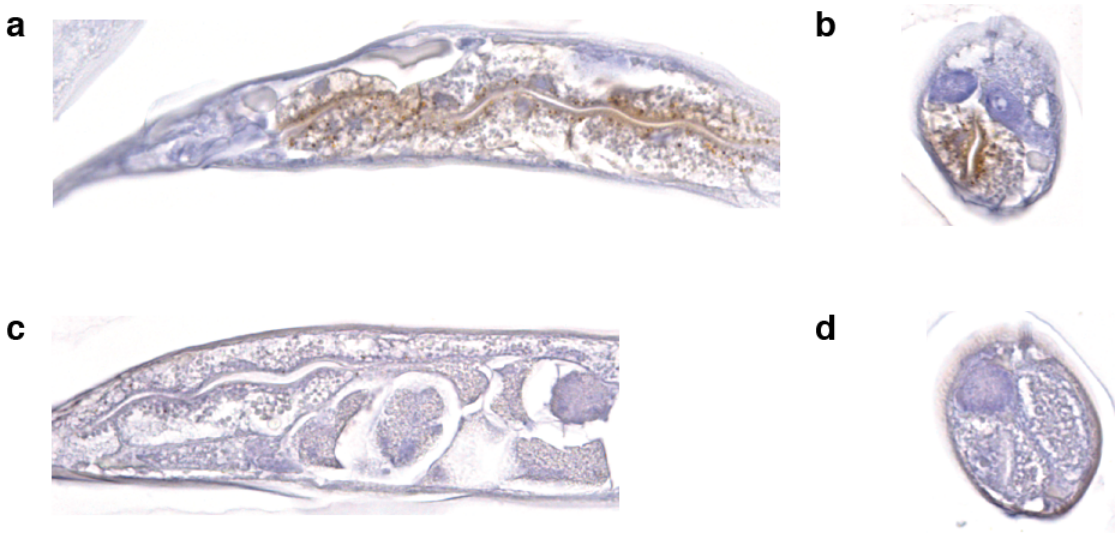

Supplementary Figure 9: Histological staining for iron (brown) in wild type (**a**,**b**) and (**c**,**d**) *ftn-2*(-);*ftn-1*(-) null adult (5-day-old). *ftn-2*(-);*ftn-1*(-) null animals have markedly reduced iron staining in the intestine. Shown are representative longitudinal and traverse cross sections.

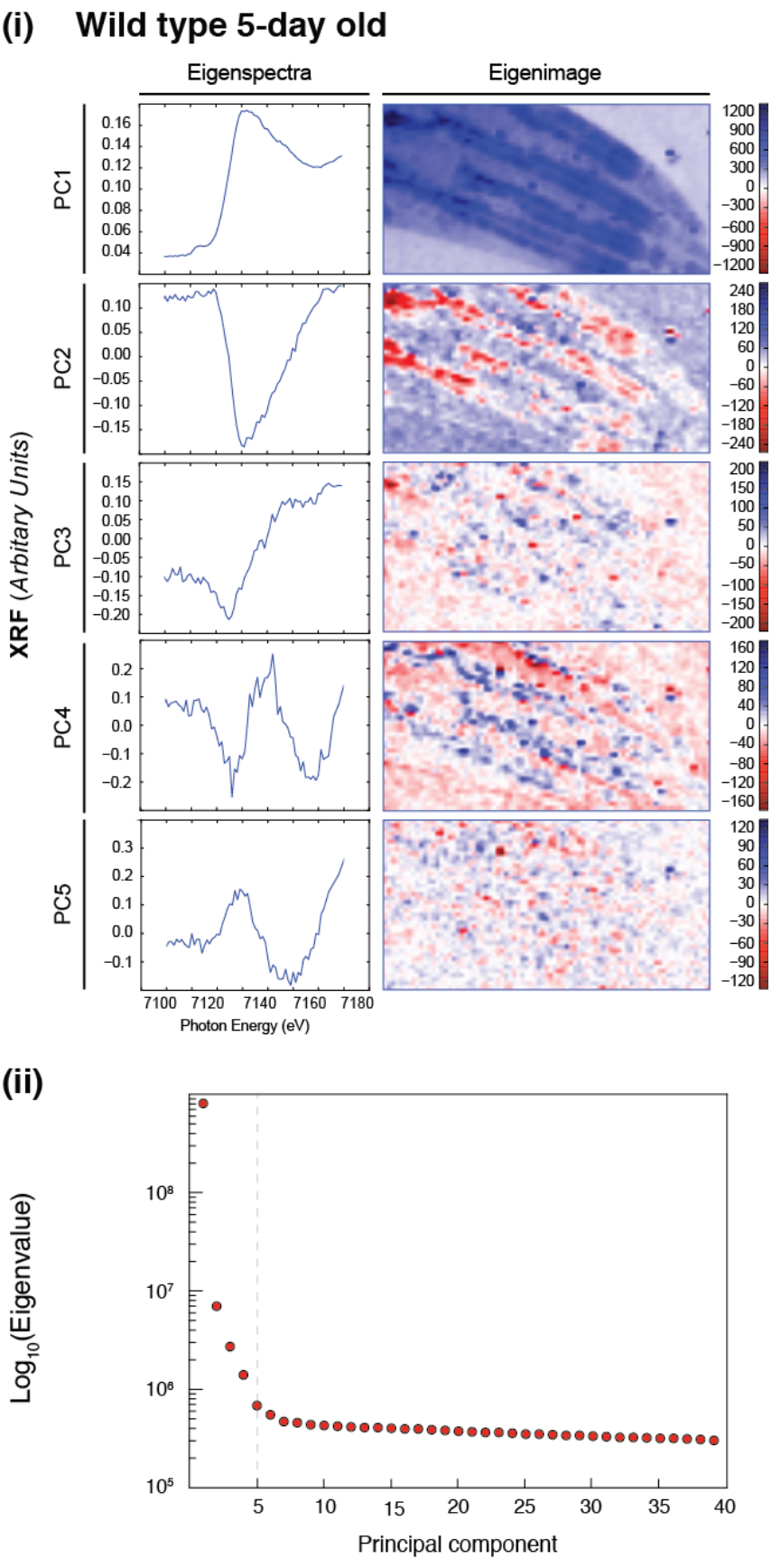
(i) Wild type 5-day old
Eigenspectra
Eigenimage
PC1
PC2
PC3
PC4
PC5
XRF (Arbitary Units)
Photon Energy (eV)
(ii)
Log10(Eigenvalue)
Principal component

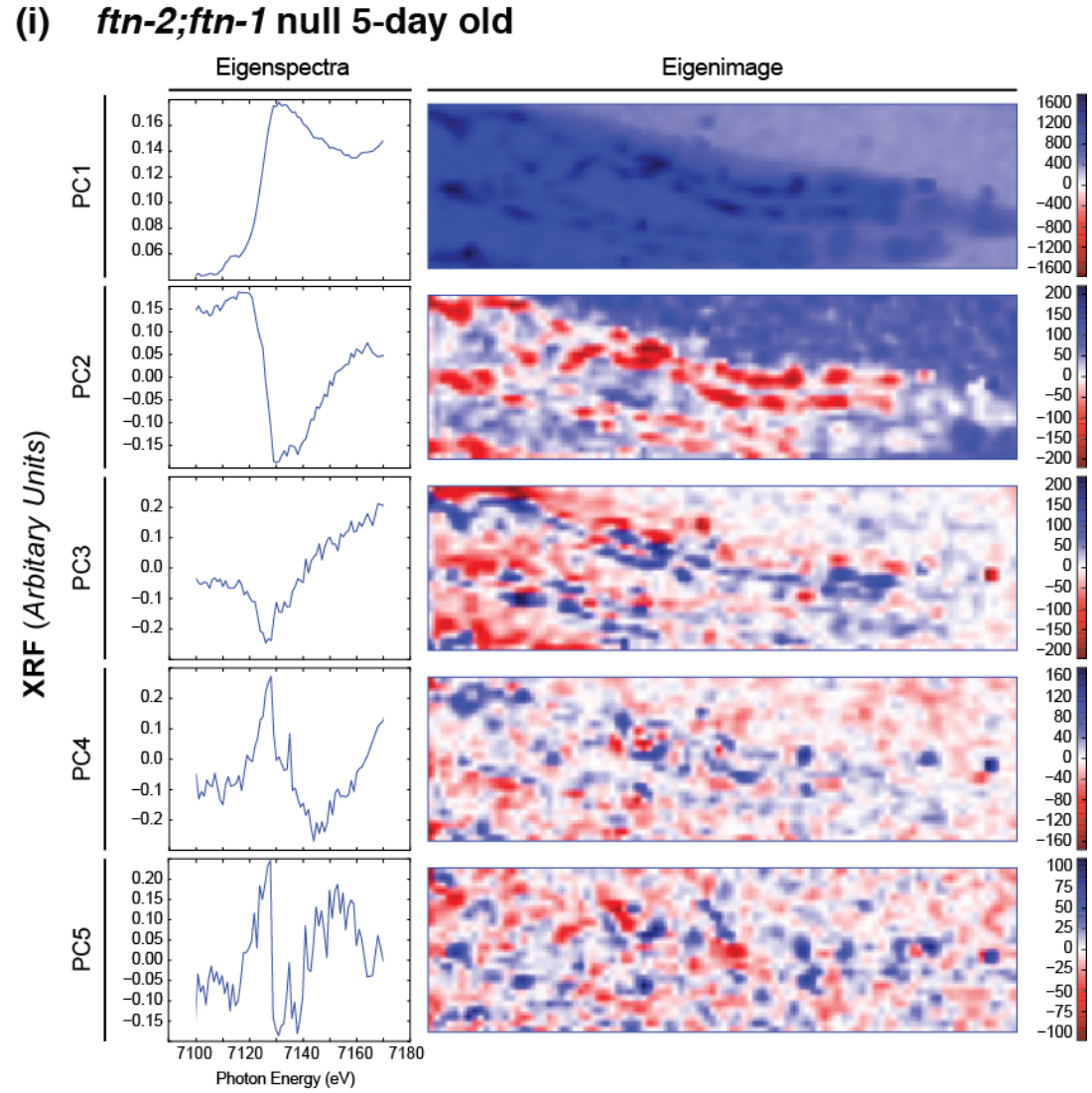
(i) ftn-2;ftn-1 null 5-day old
Eigenspectra
Eigenimage
PC1
PC2
PC3
PC4
PC5
XRF (Arbitary Units)
Photon Energy (eV)
7100 7120 7140 7160 7180

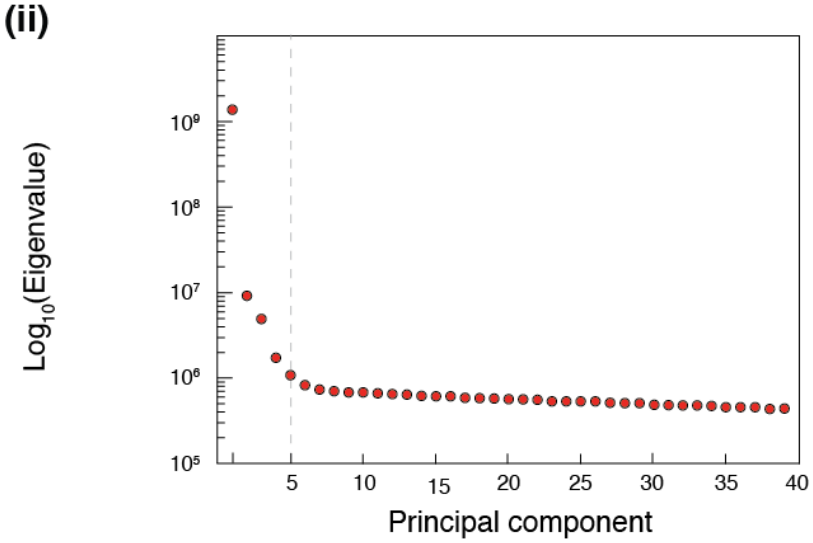
(ii)
Log10(Eigenvalue)
Principal component

(i) Wild type 12-day old

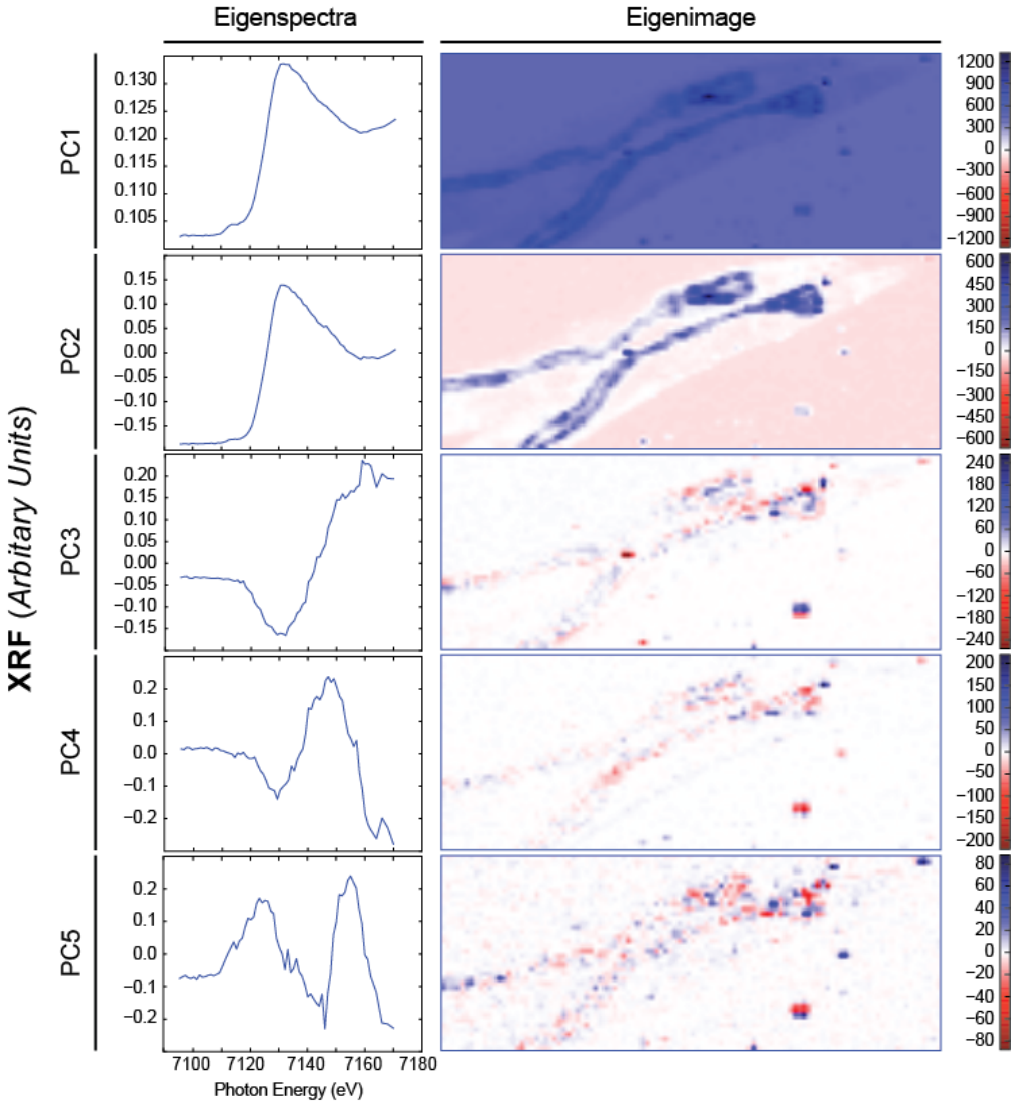

(ii)

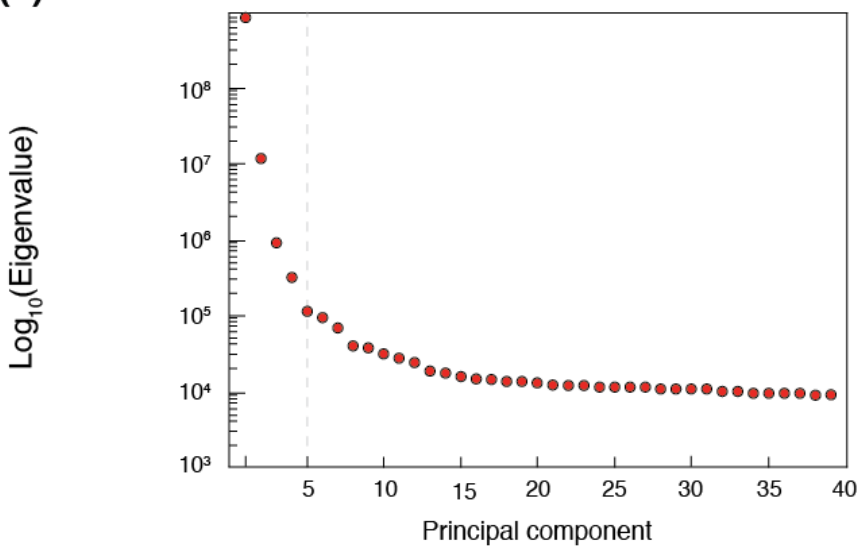

Supplementary Figure 10: (i) Principal component analysis (PCA) was used to obtain a set of abstract eigenimages and eigenspectra from the data's covariance matrix. These data provided a reduced orthogonalized search space for clustering pixels with similar spectral response in subsequent analysis. (ii) Based on the Skree plot – $\log_{10}$(eigenvalues) as a function of principal component – the first 5 components accounted for >98% of the observed variance and additional components were excluded from the analysis. (a) Wild type (WT) 5-day old; (b) *ftn-2* (-) 5-day old; and (c) WT 12-day old

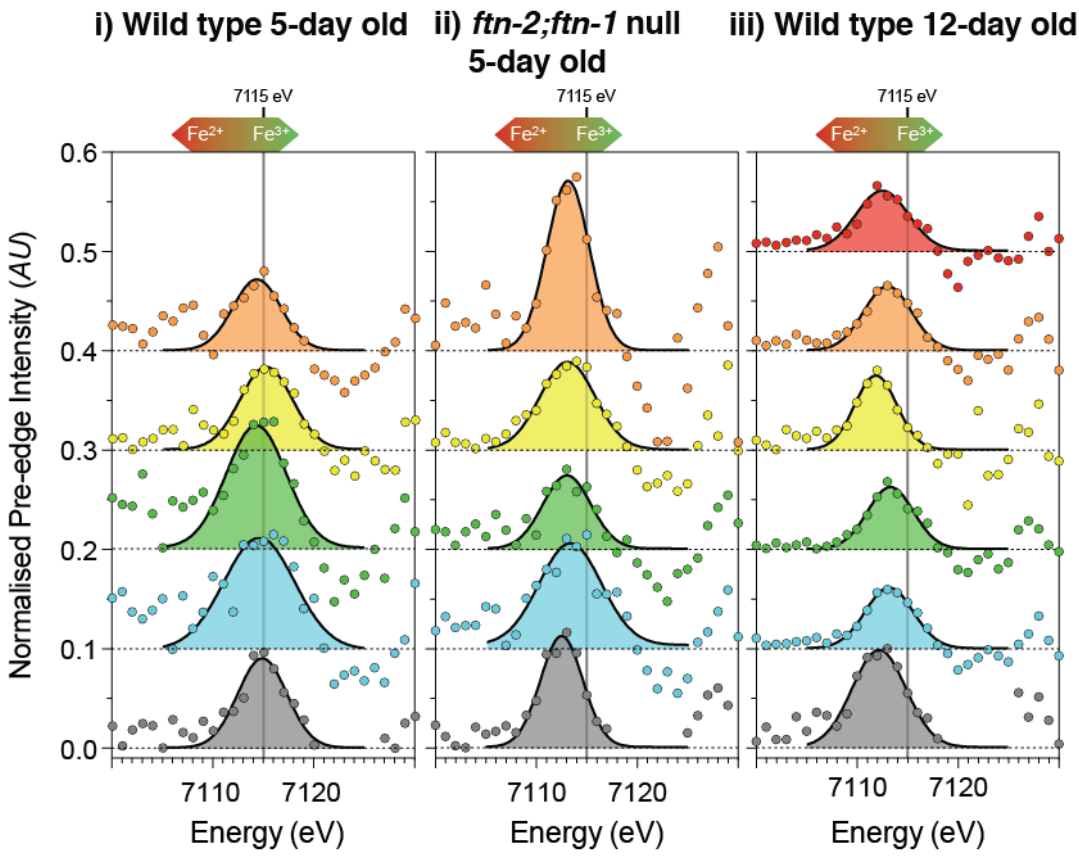

Supplementary Figure 11: The extracted 1s→3d pre-edge features (after subtraction of intensity due to the rising edge) show systematic changes in both centroid energy and intensity with the ratio of Fe^{3+}/Fe^{2+}. The raw data and fits are superimposed to emphasize the quality of the fits from which the centroid values were determined. The extracted pre-edge (circles), and Gaussian components of the fit (solid black lines), are shown for each ROI presented in Figure 5.

a

gtataatttatctcccaaaaaacacttttcaagtttataacctatatctaagtttaaaaattttgagta
caggacaagtatgagtttacgaagcatcatattaaaatcaaaatgtaatgtgaatgtggacgctagaaa
gccaggcgaaaagggacatcacacttctgcaaaaagttattttcattcggcgatccttggatgtagttt
tcttacagaaggttaagcttctcaaaatgtacttcaacacttaggtttccatattagttcattgaaacg
catgtttctgtaaacaagaacccttcgttgccaatatgtaatgtgcaaaaatcataatcagtttatca
atgatcacaatcacaaactccgccccagagttgtccagtttaaaaacacccacagtcccggacacgta
atcaagtcattatatttctgccaagtaaatcgtcATGTCTCTAGCTCGTCAAAACTATCACGATGAAG
TCGAAGCGGCCGTCAATAAACAGgtatgatcattgttttgacaaatgggaaaaatatattaggaaggtt
ggaaattgagaagagatttagaaaaagagaggatgtgtcgtgagaaaattaatcactgatgtctggtta
ctttaaattaggaatttaactgattaataaaaacattgaaacacaccacacgcttatttttccaaccgg
caacattttgttttttttaacgaacaagggcaggcagacagtacctgaagaagcgcaatttgatcatg
gcagcgtcgatgatttctttgctcttatgccagtcatccaaaaaaaatatacagaataggcggcagtag
atagacgagcacgtgagactgaaagcgtctacaataaaaatcctatctgagcttgcttttgaactggac
gaaattaacactgaaatgcttttaaaattagaagtattactcaattaaaagcttaaattacctttccag
ATTAACGTAGAACTCTACGCCTCCTATGTCTATCTATCGATGTCTGCACACTTCGATCGTGATGATATC
GCACTTCGGAACATTGCCAAATTTTTCAAGGAGCAATCGGATGAGGAGCGTGGCCATGCCACAGAGCTC
ATGAGAATTCAAGCTGTCCGTGGAGGACGTGTTGCCATGCAGAACATTCAGAAGCCAGAGAAAGACGAG
TGGGGAACTGTCCTTGAAGCATTTGAAGCCGCACTTGCTCTAGAGAGAGCCAATAATGCATCTTTGTTG
AAGCTTCATGGAATCGCCGAACAACGCAATGACGCGCACTTGACAAATTACATTCAGGAGAAGTATTTG
GAAGAGCAGgttggcattttcagtttaaactcctatttttataacgtttattaagGTACATTCGATCAA
TGAATTTGCTCGCCACATTGCAAATATCAAGAGAGCCGGCCCAGGACTCGGAGAATATTTGTTCGACAA
AGAGGAATTTTCTGATTAAtaatttttatttgatgtatttattgtacatatggatgaaattgtatattt
actgaaatgaaacacattgaaaacttcagagattagcagttcctaaaaaggttcaacctttttcaaccc
tttgtggcggaaatctgagacacataaggtgtttttaaatgtttatttggaaaaaccgttagtatatg
gaattaatacaatataagggaaatattttgtattgaagcttacaagaagctttcattgtttacagcgcc
atgtggaattctacgttttcagatgttttcccaaaaacaacataatatatttgttctgggtatatcaaa
agatttccaaaaaaattatttctaattttcaaaaaatatctctatcgatgtggaaagtgttgtagaact
taaaaaagtttctgtatactttcagacagaatttttgttttcaatggcatttttgaatgttttcataa
ccaacgtggctcaataatgtttttgaaatgcacttatgtacatttttgttcttaattatattttcaaaa
cagcttcatttctttaaataatgtgtatatttaaaaaaaaa

b

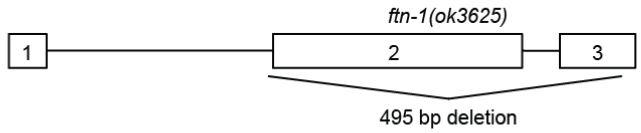

c

ATG TCT CTA GCT CGT CAA AAC TAT CAC GAT GAA GTC GAA GCG GCC GTC AAT AAA CAG gta tga
M S L A R Q N Y H D E V E A A V N K Q V *

Supplementary Figure 12: DNA sequence of the *ftn-1* locus. (**a**) Shown are intronic and untranslated sequences in lower case and exon sequence in (blue) upper case. The *ftn-1*(*ok3625*) lesion is underlined. (**b**) Schematic of the *ftn-1*(*ok3625*) deletion and (**c**) predicted 20 amino acid truncation product..

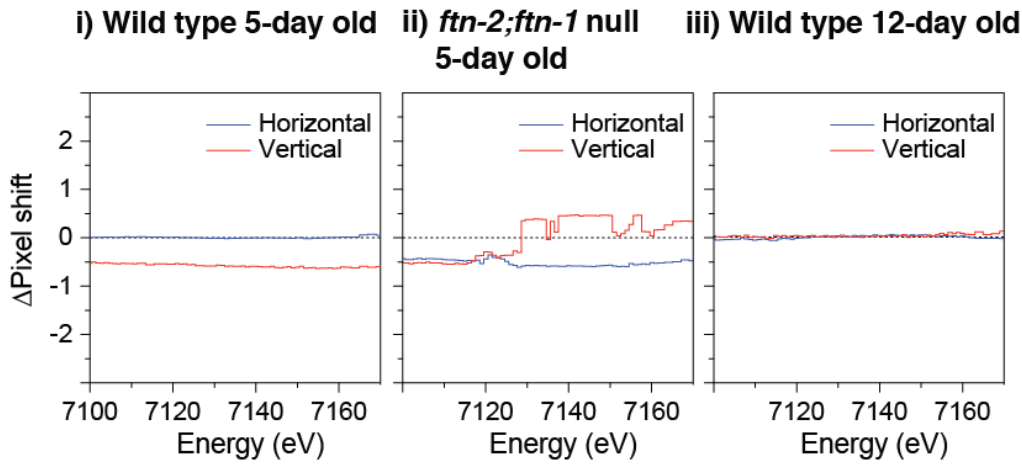

Supplementary Figure 13: The distribution of Ca was used to align each elemental micrograph prior to XANES analysis. As Ca is the most readily diffusible inorganic element and highly enriched within the intestine (along with Fe) we utilized the cross-correlation routine implemented in MANTiS to ensure major features were aligned before undertaking PCA.